

MAGNETIC FIELD TOPOLOGY IN PROMINENCES

ROBERTO LIONELLO, ZORAN MIKIĆ, AND JON A. LINKER

Science Applications International Corporation, San Diego, CA 92121-1578;
roberto.lionello@saic.com, zoran.mikic@saic.com, jon.a.linker@saic.com

AND

TAHAR AMARI

Centre de Physique Théorique, École Polytechnique, 91128 Palaiseau Cedex, France;
amari@cph.t.polytechnique.fr

Received 2002 April 16; accepted 2002 August 16

ABSTRACT

We present a study of the magnetic field lines of a prominence using MHD and thermodynamic/hydrodynamic (TH) models. Previous modeling of prominences has tended to emphasize either magnetic field modeling or TH modeling in isolation. In this paper, we combine these approaches to model a long-lived filament observed in 1996 August–September. In our new approach, we (1) use magnetograms to prescribe the boundary conditions for the magnetic flux in three-dimensional MHD simulations, (2) show that observed magnetic flux changes can produce a fluxrope and that the dipped (concave upward) portion of the field lines form in the approximate location of the observed prominence, and (3) show that TH computations, using the computed geometry of magnetic field lines that are in three-dimensional MHD equilibrium, have condensations forming in the dipped portions of the field lines.

Subject headings: MHD — Sun: corona — Sun: magnetic fields — Sun: prominences

On-line material: color figures

1. INTRODUCTION

Prominences and filament condensations have been studied for many years, yet the means by which they support cool, dense chromospheric material against gravity in the hot corona is still not understood. The coronal magnetic field is recognized as playing a crucial role in the structure of prominences. If dips (concave upward portions) are present in magnetic flux tubes of sufficient field strength, they can in principle support the dense chromospheric material present in the condensations while insulating the cool ($\sim 10^4$ K) plasma from the surrounding million degree corona.

Demonstrating a realistic, self-consistent plasma and magnetic field configuration that models a filament is a formidable problem, which couples finding a global mechanical equilibrium with determining a solution for the energetics of the fluid. It requires solving the complex thermodynamics associated with the upper chromosphere and transition region while also accurately calculating the three-dimensional magnetic field structure. Such a three-dimensional self-consistent model has not yet been attempted for even an idealized magnetic configuration, let alone one that is based on observed photospheric magnetic fields. Because the plasma β (ratio of plasma pressure to magnetic pressure) in the lower solar atmosphere is typically $\ll 1$, the thermodynamic properties of the plasma along the magnetic flux tubes can be treated separately from the force balance of the magnetic configuration. Therefore, prominence models have usually decoupled the problem and focused on one of the two main elements: (1) Finding a mechanical equilibrium, i.e., finding a magnetic configuration with the required dips (van Ballegoijen & Martens 1989; Amari & Aly 1992; Antiochos, Dahlburg, & Klimchuk 1994; Aulanier & Démoulin 1998; Amari et al. 1996, 1999; DeVore & Antiochos 2000; Aulanier, DeVore, & Antiochos 2002), and (2) studying the energetics for a given

magnetic field, i.e., showing by means of one-dimensional fluid dynamic/thermodynamic (hereafter TH) solutions that chromospheric material can be trapped in dipped field lines and held there to form a condensation (Poland & Mariska 1986; Mok, Schnack, & Van Hoven 1991; Antiochos & Klimchuk 1991; Antiochos et al. 1999; Dahlburg, Antiochos, & Klumchuk 1998). However, these studies did not use a magnetic field in MHD equilibrium, which is what we would like to address in this paper.

Three-dimensional magnetic field configurations fulfilling condition 1 have been suggested as occurring in two principal ways: (1) concentrated shearing of a magnetic flux distribution along the neutral line, resulting in an equilibrium with dipped field lines (Antiochos et al. 1994), and (2) formation of magnetic flux rope configurations either by magnetic flux cancellation (van Ballegoijen & Martens 1989; Amari et al. 1996, 1999) or emergence of a flux rope from below the photosphere (van Ballegoijen & Martens 1990). Both of these configurations fulfill several of the theoretical and observational requirements, such as twist, shear along the neutral line, and dips (Martin & Echols 1994; Martin & McAllister 1997; Démoulin & Klein 2000). Lites et al. (1995) have described observations consistent with the flux rope picture of prominences. We note that the requirement of dipped field lines has been questioned by some observations and models (Zirker, Engvold, & Martin 1998; Antiochos, MacNeice, & Spicer 2000; Karpen et al. 2001).

A number of authors have solved the coupled TH along a magnetic flux tube to demonstrate that condensations can indeed form in dipped field lines (Poland & Mariska 1986; Mok et al. 1991; Antiochos & Klimchuk 1991; Antiochos et al. 1999; Dahlburg, Antiochos, & Klumchuk 1998). These calculations assume an idealized magnetic flux tube with a concave upward portion in the center but do not correspond to a global mechanical equilibrium.

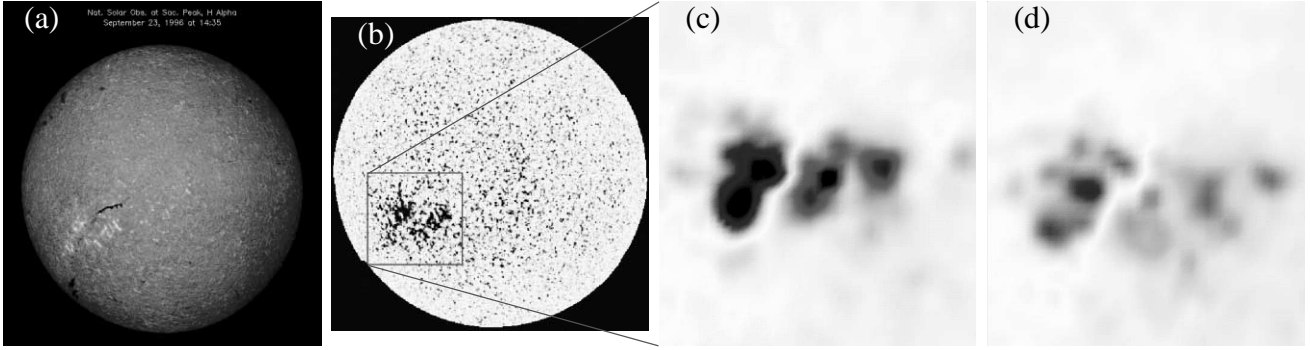


FIG. 1.—(a) $H\alpha$ image from NSO Sacramento Peak showing a filament on 1996 September 23 at 14:35 UT. (b) NSO Kitt Peak Magnetogram for 1996 September 23 (start time 17:32 UT, stop time 18:26 UT). (c) Initial flux distribution for the calculation. It was extracted and smoothed from an NSO Kitt Peak Synoptic Magnetogram for CR 1913 (the active region was observed around 17:20 UT on 1996 August 29). (d) Final flux distribution derived from the NSO Kitt Peak Synoptic Magnetogram for CR 1914 (observed around 23:57 UT on 1996 September 25). [See the electronic edition of the *Journal* for a color version of this figure.]

In this paper, we combine the two approaches described above to further investigate flux ropes as a candidate structure for prominences. First, we extend the work of Amari et al. (1999, 2000) to a more realistic situation by showing how observed changes in line-of-sight magnetograms can lead to the formation of a flux rope. In the period under examination, late summer of 1996, a prominence was seen (see Fig. 1a). The active region associated with the prominence has been studied by Mandrini et al. (2000). We use a three-dimensional MHD algorithm and specify as boundary conditions the magnetic flux obtained from the magnetograms. As the surface flux undergoes dispersal and cancellation, a flux rope is formed. We plot the dipped portions of the magnetic field and compare them with the position of the filament, as observed in $H\alpha$. In order to show that the flux rope can support the cold and dense material that is characteristic of a prominence, we use the actual magnetic field lines extracted from the final state of the three-dimensional MHD simulation to prescribe the flux-tube geometry for the computation of one-dimensional TH steady-state solutions. The use of these data in the TH model represents an innovation in respect to past works that used more idealized field models (Poland & Mariska 1986; Mok, Schnack, & Van Hoven 1991; Antiochos & Klimchuk 1991; Antiochos et al. 1999; Dahlburg, Antiochos, & Klumchuk 1998). In the limit where the plasma β is low and the magnetic pressure substantially exceeds the gravitational forces acting on the condensations, these one-dimensional solutions should closely coincide with a fully consistent thermodynamic MHD simulation. We find that the plasma and magnetic field of our solutions do indeed satisfy these criteria.

2. THE MHD MODEL AND SIMULATIONS

Our approach is based on two separate steps. We first use a three-dimensional MHD model to obtain a magnetic configuration containing a magnetic flux rope. Section 2.1 briefly describes the MHD model used for the calculations, and § 2.2 discusses the results. In § 3 we describe how we obtain TH solutions along selected magnetic field lines from the three-dimensional magnetic configuration obtained in § 2.2 and show results for both helical and arcade-like field lines.

2.1. The MHD Model

To model magnetic structures in active regions, we solve a simplified form of the MHD equations in Cartesian geometry:

$$\nabla \times \mathbf{B} = \frac{4\pi}{c} \mathbf{J}, \quad (1)$$

$$\nabla \times \mathbf{E} = -\frac{1}{c} \frac{\partial \mathbf{B}}{\partial t}, \quad (2)$$

$$\mathbf{E} + \frac{\mathbf{v} \times \mathbf{B}}{c} = \eta \mathbf{J}, \quad (3)$$

$$\rho \left(\frac{\partial \mathbf{v}}{\partial t} + \mathbf{v} \cdot \nabla \mathbf{v} \right) = \frac{1}{c} \mathbf{J} \times \mathbf{B} + \nabla \cdot (\nu \rho \nabla \mathbf{v}), \quad (4)$$

where \mathbf{E} and \mathbf{B} are the electric and magnetic fields, respectively, \mathbf{v} is the plasma velocity, c is the speed of light, η is the resistivity, ν is the viscosity, and ρ is the plasma density, assumed to be constant. The exclusion of the pressure gradient and gravity from the momentum equation is justified because the dynamics of an active region is dominated by the strong magnetic field; i.e., the corona is a low- β medium (where β is the ratio of the plasma and magnetic pressures). When equations (1)–(4) are integrated to steady state, the solution represents a force-free, nonconstant α solution for a given set of boundary conditions. For the calculation shown in § 2.2, we used an $85 \times 81 \times 81$ nonuniform grid to mesh a cubic domain, of $2 R_{\odot}$ side. The Lundquist number S is defined as the ratio of the resistive diffusion time $\tau_R = 4\pi L^2 \eta^{-1} c^{-2}$ to the Alfvén time $\tau_A = L/V_A$ (with a typical number density of $n \sim 2 \times 10^{11} \text{ cm}^{-3}$ and magnetic field of $|\mathbf{B}| \sim 100 \text{ G}$, $V_A \sim 500 \text{ km s}^{-1}$). If we consider the typical length scale in our model to be $L \sim 0.25 R_{\odot}$, we have $S \sim 1.25 \times 10^5$, which is much lower than the value in the solar corona. This is necessary to dissipate structures that cannot be resolved, since they are smaller than the cell size. However, it does not influence the large-scale dynamics in which we are interested. For the same reason, we choose ν such that the ratio of the viscous dissipative time versus the Alfvén time is $\tau_{\nu}/\tau_A = 100$.

2.2. Flux Rope Formation

Our goal is to extend the Amari et al. (2000) work to develop a more realistic configuration. Therefore, we have

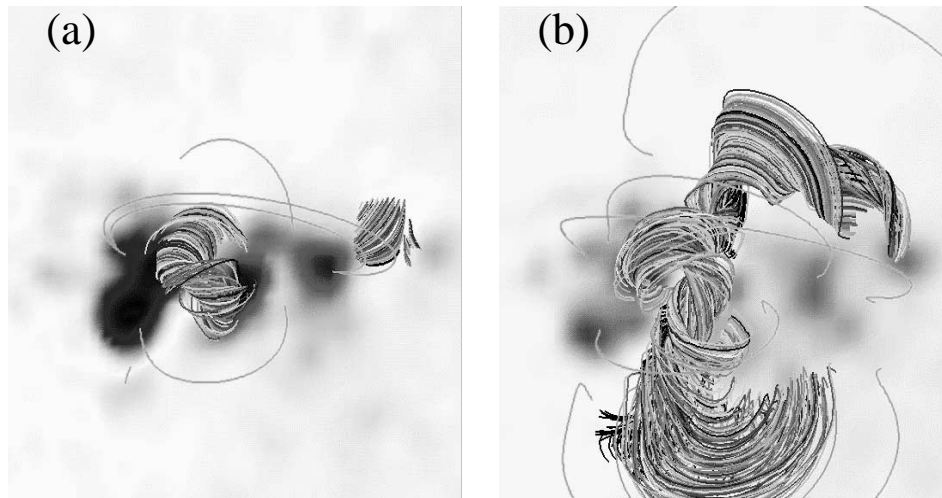


FIG. 2.—Results from the MHD calculation of the prominence magnetic field. (a) A twisted magnetic field with the initial flux distribution. (b) The magnetic flux evolves to the new state during the MHD calculation, forming a magnetic flux rope. Arcade-like field lines surround the flux rope. [See the electronic edition of the Journal for a color version of this figure.]

used line-of-sight magnetograms from NSO Kitt Peak to specify the initial and final states of the photospheric magnetic field for an MHD computation. The magnetograms correspond to the location of a long-lived filament observed in 1996 August–September (Fig. 1). The magnetogram for the initial state was taken on 1996 August 29 (Fig. 1c), and the magnetogram for the final state was taken on 1996 September 23 (Fig. 1d). The filament was associated with a decaying active region; the spreading and reduction in magnitude that occurred between the initial and final states can be seen.

The MHD computation is initialized with a potential field corresponding to the initial magnetic flux distribution. Filament magnetic fields are nearly aligned with the filament channel (Martin, Bilimoria, & Tracadas 1994; Martin & Echols 1994), indicating a highly sheared configuration. Unfortunately, because there is no suitable vector magnetograph data available at this time, we have had to impose shear in the field in an ad hoc way. To develop shear and twist in the MHD solution, we apply flows localized along the neutral line to twist the magnetic field in the initial state. The form of the shear is

$$\mathbf{v}_b = \nabla \times \psi(x, y) \hat{z}, \quad (5)$$

where ψ is a specified scalar function. If we choose $\psi = \psi(B_z)$, it can be shown that the flow derived from equation (5) preserves the original magnetic flux of the configuration (Amari et al. 1996). The corresponding flow consists of two vortices rotating in the same direction and centered on the opposite polarity regions. The maximum speed of the flow is set to one hundredth of the Alfvén speed. For $0 \leq t < 15\tau_A$, the system evolves through a series of force-free, increasingly sheared equilibria. These flows are not meant to represent a physical process; they are just a convenient way of developing the strong shear along the neutral line that is observed in filaments (Fig. 2a). In actuality, the shear and twist may emerge with the magnetic field when the active region is born (Leka et al. 1996).

Amari et al. (2000) and Linker et al. (2001) have shown how magnetic flux cancellation in a sheared arcade leads to

formation of a flux rope. For $15\tau_A \leq t \leq 45\tau_A$, we apply an electric field at $z = 0$ to evolve the photospheric magnetic flux from the initial state to the final state, as described in Linker et al. (2001). Cancellation of magnetic flux in this more realistic configuration results in the formation of a complicated flux-rope structure (Fig. 2b), surrounded by arcade-like field lines. The magnetic field in the flux rope has dips; we will show how the cold and dense material typical of a prominence can be stored there.

3. DIPS AND CONDENSATIONS

In § 2.2 we have obtained the magnetic field with the three-dimensional MHD model. A selection of helical field lines extracted from the MHD simulation is presented in Figure 3. They show a wide variety of shapes. Some field lines feature more than one dip. The dips are not always located at the field line midpoint. In order to see whether the helical field lines can support a prominence, we show that at

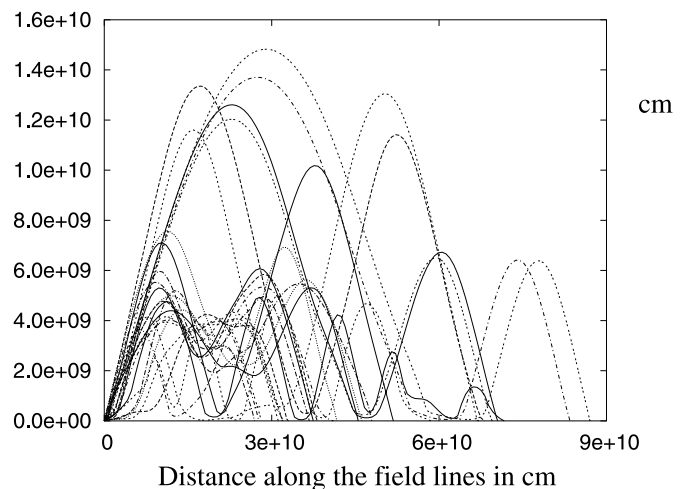


FIG. 3.—Height profile as a function of the distance along the field line for magnetic field lines with dips. Some field lines have more than one dip.

least a steady state solution with a condensation is possible in dipped field lines. We now proceed to find the plasma properties, ρ and T , along selected field lines with a one-dimensional TH model. This can be done because the plasma β is low (an a posteriori check yields $\beta \lesssim 10^{-4}$), moves only along the field lines, and the perturbation to \mathbf{B} due to pressure gradients is small. The effect of gravity on the magnetic field dynamics is negligible as well,

$$\beta_g \sim \frac{\rho g z}{B^2 / (8\pi\rho)} \lesssim 10^{-4}, \quad (6)$$

where g is the gravitational acceleration and z is the height above the solar surface. We solve the following equations:

$$\frac{\partial \rho}{\partial t} + v \frac{\partial \rho}{\partial s} = -\rho \frac{1}{A} \frac{\partial}{\partial s} A v, \quad (7)$$

$$\begin{aligned} \frac{\partial T}{\partial t} + v \frac{\partial T}{\partial s} = & -(\gamma - 1)T \frac{1}{A} \frac{\partial}{\partial s} A v + (\gamma - 1) \frac{m_p}{k\rho} \\ & \times \left[\frac{1}{A} \frac{\partial}{\partial s} A \kappa_0 T^{5/2} \frac{\partial T}{\partial s} - n_e n_p Q(T) + H \right], \quad (8) \end{aligned}$$

$$\frac{\partial v}{\partial t} + v \frac{\partial v}{\partial s} = -\frac{1}{\rho} \frac{\partial p}{\partial s} - g_s + \frac{1}{\rho A} \frac{\partial}{\partial s} A \left(\nu \rho \frac{\partial v}{\partial s} \right), \quad (9)$$

where s is the length element along the field line, T , p , and ρ are the plasma temperature, pressure, and density, k is Boltzmann's constant, $A(s) \propto 1/B(s)$ is the expansion factor of the field line, κ_0 is Spitzer coefficient for thermal conduction ($\kappa_{\parallel} = \kappa_0 T^{5/2}$), $\gamma = 5/3$ is the ratio of specific heats, Q is the radiation loss function (Athay 1986), n_e and n_p are the electron and proton number density and are equal in our calculation, $H = H_0 \exp[-(r - R_{\odot})/\lambda]$ is a parameterized heating function, $g_s = \mathbf{g} \cdot \mathbf{B}/B$ is the projected gravitational acceleration, m_p is the proton mass, and $\rho = m_p n_p$.

For our choice of length scale $\lambda = 0.05 R_{\odot}$, the heating at the base (H_0) is chosen to give a surface energy flux of $4.6 \times 10^5 \text{ ergs cm}^{-2} \text{ s}^{-1}$. According to Rosner, Tucker, & Vaiana (1978), in the case of symmetric, low-lying (constant pressure) loops, there exists a lower limit L_H for the length scale λ of an exponentially decaying heating function in order to have a solution with maximum temperature in the middle. This limit is proportional to the length of the loop L . Vesecky, Antiochos, & Underwood (1979) criticized the stability analysis of Rosner et al. (1978), arguing that having the maximum T in the middle is not a necessary condition for stability. However, numerical simulations confirmed the existence of a length limit (Serio et al. 1981); when $\lambda < L_H$, only a solution with a temperature minimum in the middle is possible. The presence of a condensation in the middle can be thought as splitting the loop into two loops, each of length $L/2$. This effectively decreases L_H to $L_H/2$, and if $\lambda > L_H/2$, then the solution with condensation in the middle is stable. In our simulations, we use a heating scale in height rather than along the loop; the loops can be asymmetric, and this stability argument can only be applied heuristically. However, it is important to note that there are strong indications from our one-dimensional TH simulations and those of others (Antiochos et al. 2000; Karpen et al. 2001) that it is not always possible to obtain steady state solutions for an arbitrary choice of heating profile. In fact, the nonsteady solutions may explain flows and time-dependent behavior of observed filaments (see below).

As an initial state, we choose a smooth temperature profile ranging from $T = 2 \times 10^4 \text{ K}$ at the boundaries to

$T = 4 \times 10^5 \text{ K}$ at the center of the loop and calculate the corresponding pressure and density from solving the hydrostatic equilibrium equation. The initial temperature is chosen such that the system is thermally unstable. Equations (7)–(9) are advanced to steady state using characteristic boundary conditions, zero heat flux, and a fixed density ($5 \times 10^{10} \text{ cm}^{-3}$) at the ends of the loops. With these boundary conditions at $s = 0$ and $s = L$, a dense and cold chromosphere is formed, next to a transition region with sharp gradients. In the interior, we have a hot, tenuous corona. Two kinds of physical, stable solutions are possible: with and without condensation. Loops with a height profile, as in Figure 4a, do not support a condensation. In fact, an eventual condensation forming at the top of the loop would be unstable to the Rayleigh-Taylor instability (dense material on top of tenuous). The solution is the classical loop solution, with temperature maximum and density minimum at the top (Figs. 4b and 4c). These loops constitute the arcade surrounding the flux rope, and, in particular, the loop in Figure 4 overlies the location of a dip. When a dip is present in the magnetic field line (i.e., if a field line belongs to the flux rope), as in Figure 5a, there is a local gravitational energy minimum. This means that this configuration allows stable solutions both with and without condensation. By starting from a hydrostatic equilibrium and using a heating function concentrated at the base (Aschwanden, Nightingale, & Alexander 2000; Aschwanden, Schrijver, & Alexander 2001), we obtain a condensation in the dip (Figs. 5b and 5c). The loop in Figure 5 is fairly symmetric around the midpoint and has only one dip. This is not a general feature. In Figure 6, we show a TH simulation for a clearly asymmetric field line with a dip where a condensation is formed. Figure 7 shows results for a field line with two dips and two condensations. We have verified that small variations of the parameters still produce solutions with condensations. For a choice of parameters radically different from ours, solutions without a condensation are possible.

The magnetic field dips can be used as a proxy for the location of filament material (Aulanier, Srivastava, & Martin 2000). In Figure 8a we have plotted the dipped portion of the field lines. This can be compared with $H\alpha$ observations of the filament at different instants in times (Figs. 8b–8g). The location of the filament roughly corresponds with the location of magnetic dips. However, the shape and intensity of the filament show evidence of time-dependent behavior. In particular, the section of the filament between the two poles of the active region almost disappears and reappears over time. Our steady state model obviously cannot reproduce this evolution. Projection effects can also account for some differences in shape. We do not attempt to model barbs, since the parasitic polarities to which they are associated are present at length scales smaller than in the present simulation.

In Figure 9 we show side views of the magnetic dips at different stages of the simulation, seen from the side. As the magnetic flux evolves and is dispersed, the dips raise, and the cold and dense chromospheric material stored therein is lifted into the corona. This phase is a precursor to eruption (Amari et al. 2000; Linker et al. 2001).

4. CONCLUSIONS

We have shown how changes in the observed photospheric magnetic flux in a sheared magnetic configuration

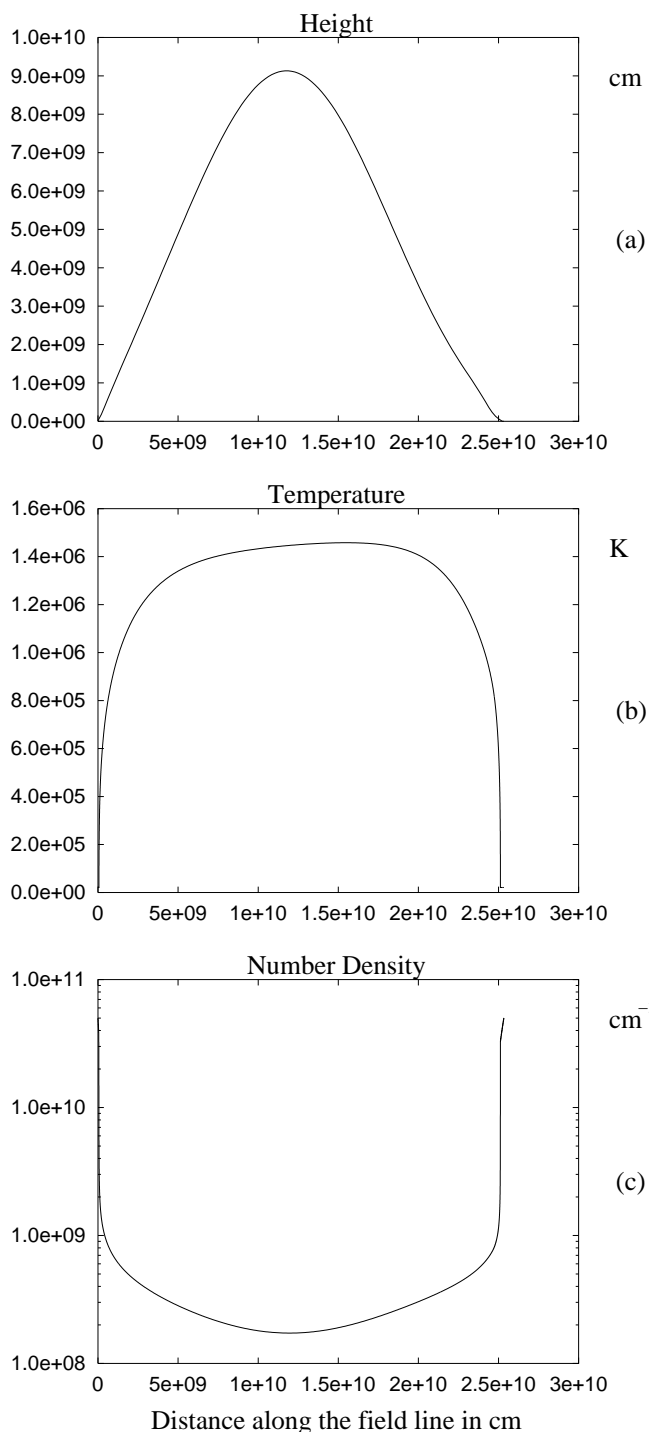


FIG. 4.—(a) Height profile as a function of the distance along the field line for an arcade field line that cannot develop a stable condensation. (b) Temperature profile. (c) Density profile. Notice that no dip is present to sustain an eventual condensation.

can lead to the formation of a magnetic flux rope. Solutions of the hydrodynamic equations with thermal conduction, heating, and radiation losses were performed along the field lines of the final state of our MHD equilibrium.

They show that the dips in the magnetic field lines in the flux rope can support the dense and cold material typical of a prominence. Arcade-like field lines do not have dips and are therefore incapable of confining the heavy material

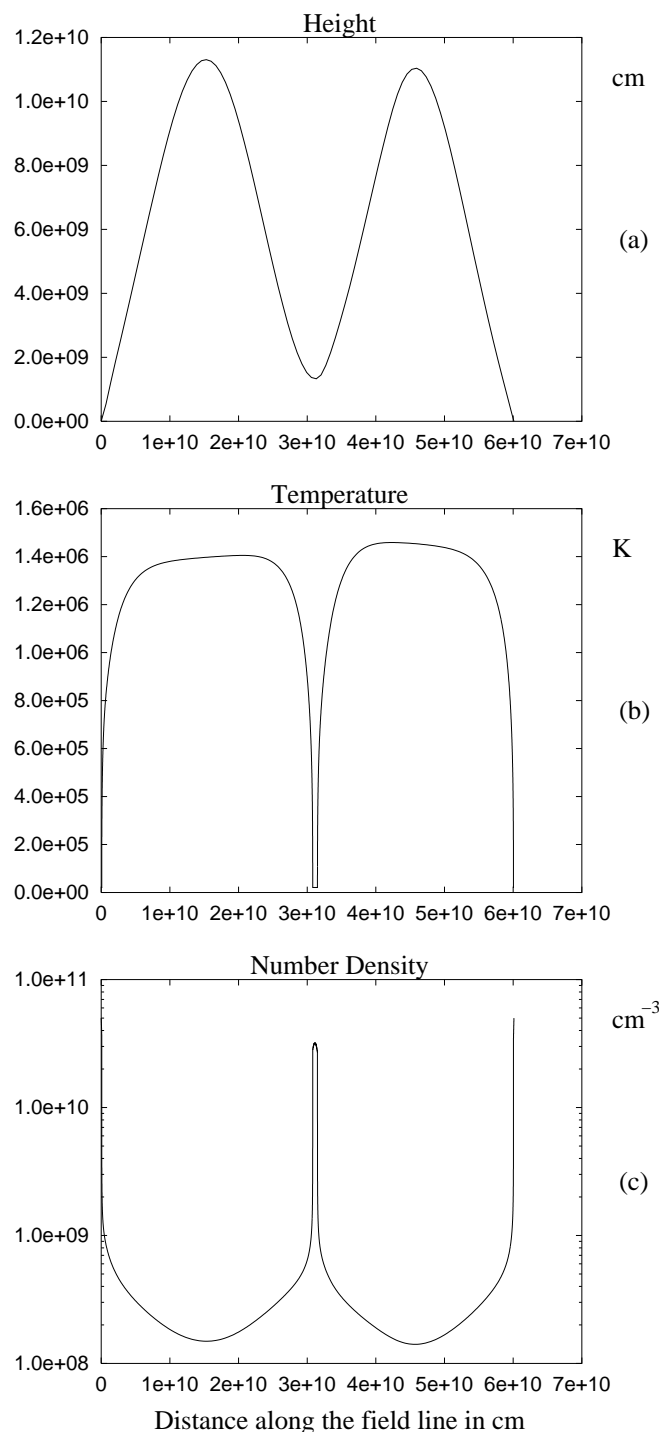


FIG. 5.—(a) Height profile as a function of the distance along the field line for a flux rope field line that develops a condensation. (b) Temperature profile. (c) Density profile. The condensation appears in the dip of the field line. For a more asymmetric case, see Fig. 6.

against gravity. For the sake of simplicity, we have used a simple parametric heating function and investigated only steady state solutions. Because we have looked for steady states for the MHD and TH models, the timescales of the two models are decoupled. Finding steady state solutions is sufficient to verify that our MHD equilibrium can support a prominence. However, steady state should not be considered a necessary condition to represent prominences. In

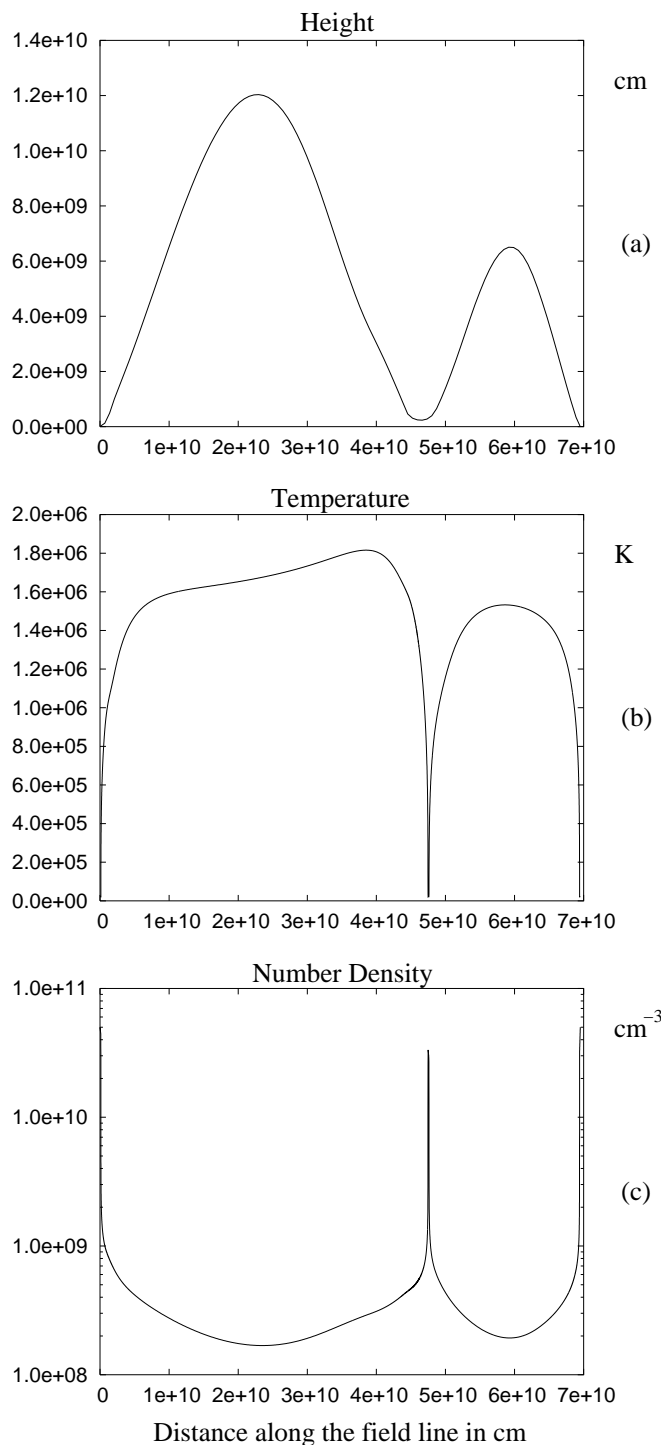


FIG. 6.—(a) Height profile as a function of the distance along the field line for a flux rope field line that develops a condensation. (b) Temperature profile. (c) Density profile. The condensation appears in the dip of the field line. For a more symmetric case, see Fig. 5.

particular, our work does not contradict a dynamic interpretation of the nature of a condensation (Karpen et al. 2001), which may explain the time-dependent behavior of long-lived filaments that appear and disappear over time. Furthermore, we cannot exclude that using a heating function as in Karpen et al. (2001) may form unsteady condensations in both dipped and undipped field lines. The location of the dips roughly corresponds to the position of the prom-

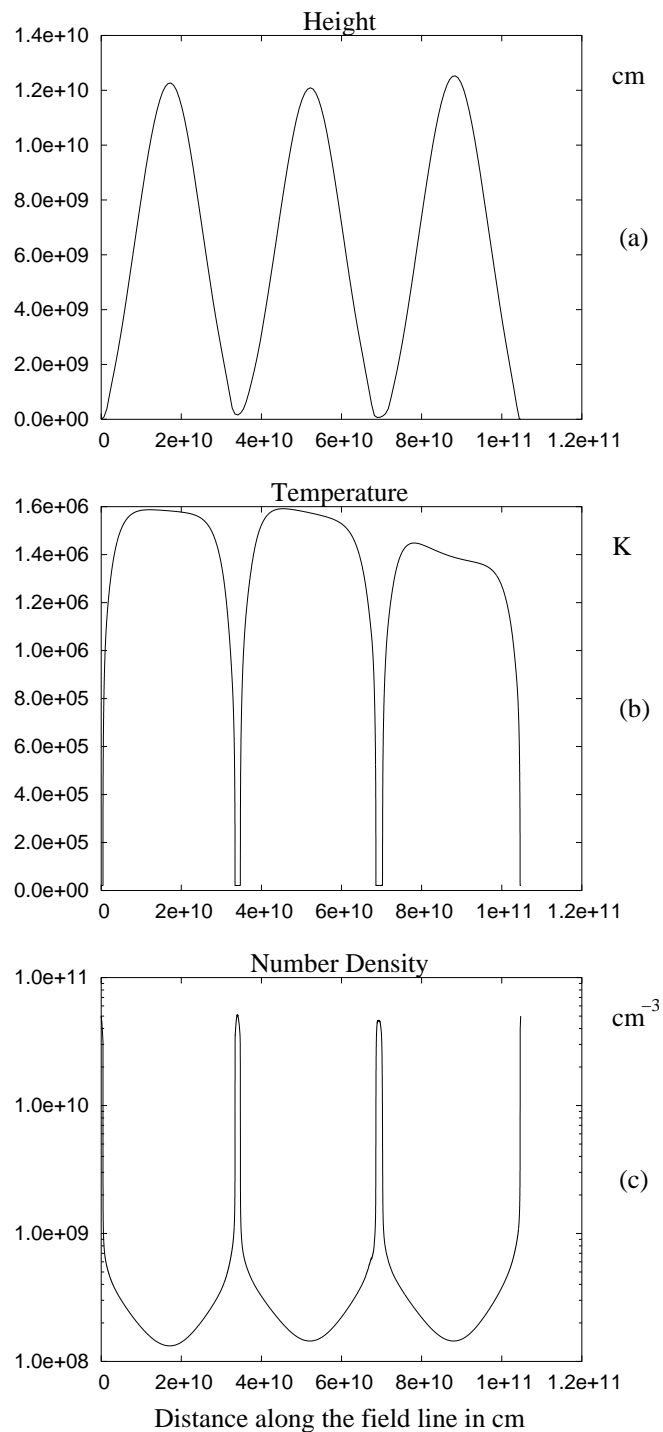


FIG. 7.—(a) Height profile as a function of the distance along the field line for a flux rope field line that develops two condensations. (b) Temperature profile. (c) Density profile. The condensations appear in the dips of the field line.

inence observed in 1996 August–September. Of course, our calculation can only be regarded as suggestive. We do not have data for the actual sequence of magnetic flux changes associated with the filament's formation, and the actual transverse field along the filament channel is unknown.

We also have not addressed the point of how the prominence is actually formed, either via evaporation and successive condensation of chromospheric material, or

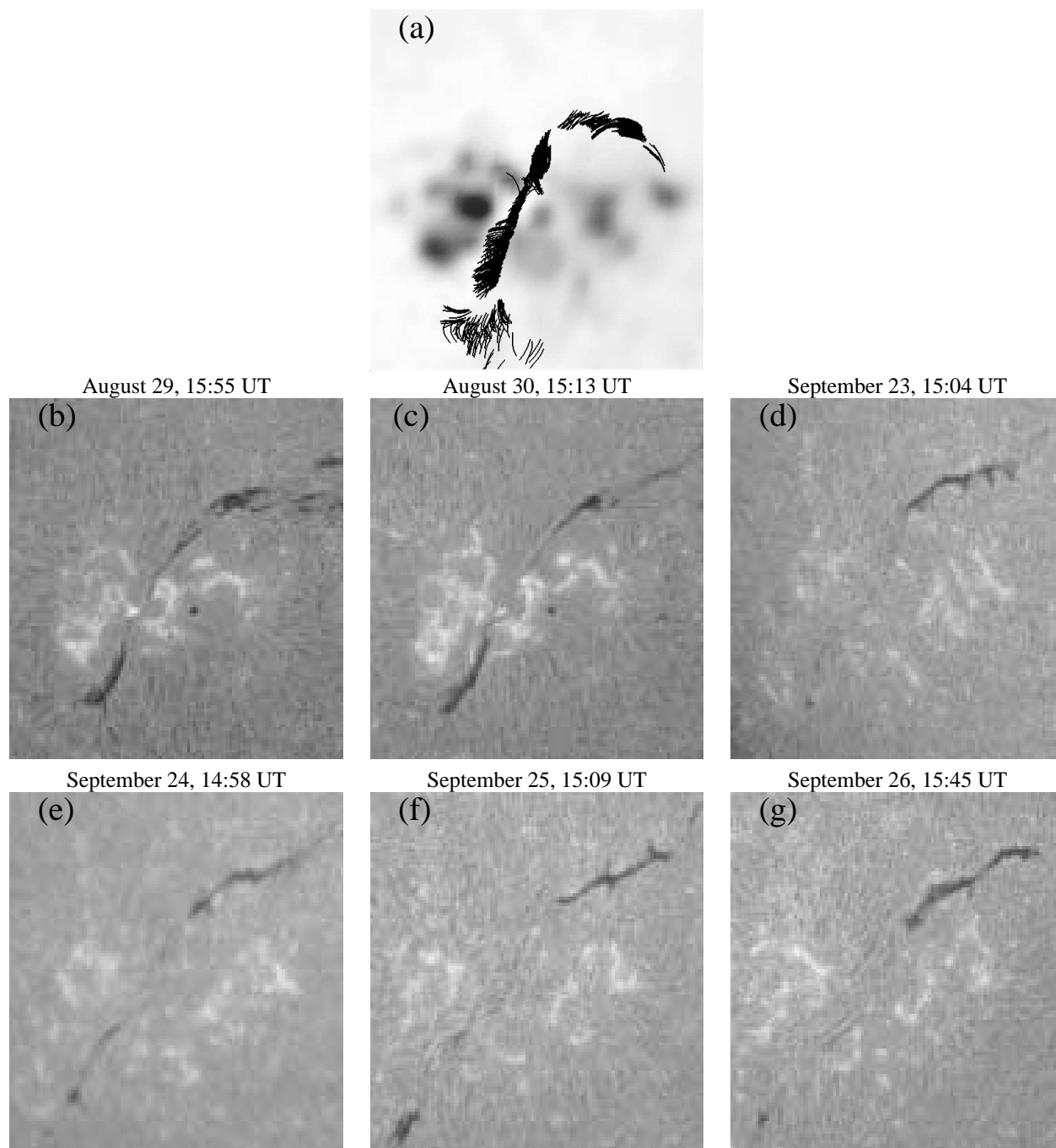


FIG. 8.—(a) Location of the concave upward portions of the magnetic field lines (magnetic dips). These are the places where filament material is more likely to reside. Actual filament location in the Sacramento Peak $H\alpha$ images for comparison: (b) August 29, 15:55 UT; (c) August 20, 15:13 UT; (d) September 23, 15:04 UT; (e) September 24, 14:58 UT; (f) September 25, 15:09 UT; (g) September 26, 15:45 UT. [See the electronic edition of the *Journal* for a color version of this figure.]

through mechanical lifting of cold and dense matter during the reconnection phase. However, the raising of magnetic dips in response to the evolution of the surface flux is compatible with the latter, although it does not exclude the former. In order to investigate this issue, a more sophisticated model is needed. In the future, we plan to conduct a self-consistent three-dimensional MHD simulation with an energy equation incorporating coronal heating, thermal conduction, and radiation losses to study this effect.

We thank Yung Mok for helpful discussions. The authors gratefully acknowledge the support of the National Aeronautics and Space Administration (Sun-Earth Connections Theory Program and Supporting Research and Technology Programs) and the National Science Foundation (Space Weather Program ATM 9613834) in undertaking this study. We also thank the San Diego Supercomputer Center and the National Energy Research Supercomputer Center for providing computational support.

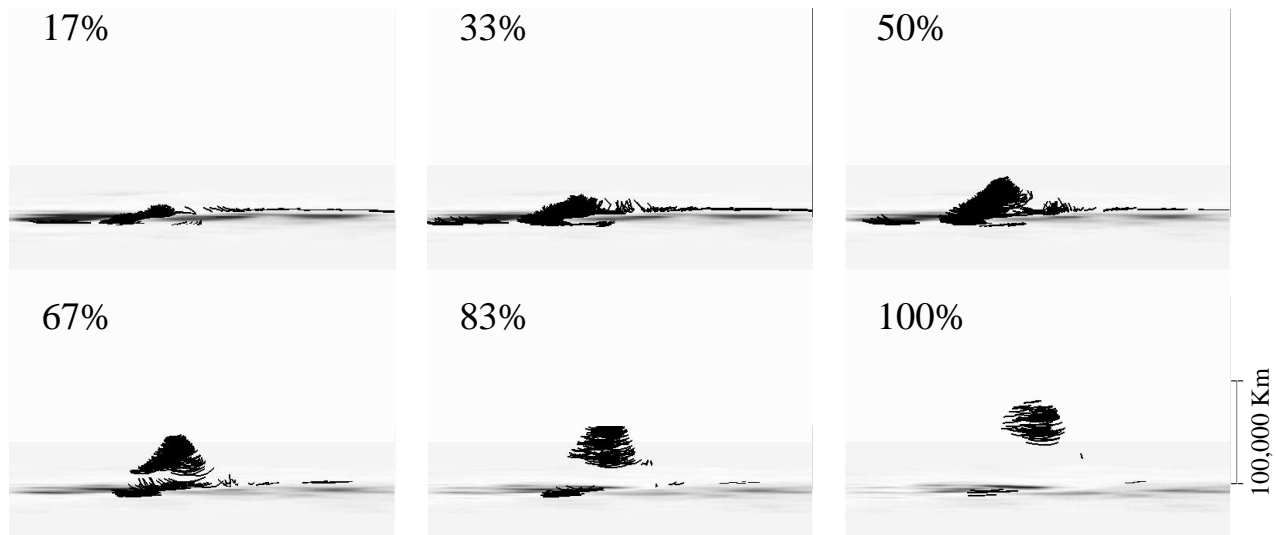


FIG. 9.—Evolution of the concave upward portion of the magnetic field (dips) during the MHD calculation viewed from the side. The planes are colored according to the intensity of the magnetic flux. The percentage of emerged flux is shown in the top left corner of each image. The dips rise as the surface magnetic field evolves from the configuration, as in Fig. 1c to that in Fig. 1d. [See the electronic edition of the Journal for a color version of this figure.]

REFERENCES

- Amari, T., & Aly, J. J. 1992, *A&A*, 265, 791
 Amari, T., Luciani, J. F., Aly, J. J., & Tagger, M. 1996, *ApJ*, 466, L39
 Amari, T., Luciani, J. F., Mikić, Z., & Linker, J. 1999, *ApJ*, 518, L57
 ———. 2000, *ApJ*, 529, L49
 Antiochos, S. K., Dahlburg, R. B., & Klimchuk, J. A. 1994, *ApJ*, 420, L41
 Antiochos, S. K., & Klimchuk, J. A. 1991, *ApJ*, 378, 372
 Antiochos, S. K., MacNeice, P. J., & Spicer, D. S. 2000, *ApJ*, 536, 494
 Antiochos, S. K., MacNeice, P. J., Spicer, D. S., & Klimchuk, J. A. 1999, *ApJ*, 512, 985
 Aschwanden, M., Nightingale, R. W., & Alexander, D. 2000, *ApJ*, 541, 1059
 Aschwanden, M., Schrijver, C. J., & Alexander, D. 2001, *ApJ*, 550, 1036
 Athay, R. G. 1986, *ApJ*, 308, 975
 Aulanier, G., & Démoulin, P. 1998, *A&A*, 329, 1125
 Aulanier, G., DeVore, C. R., & Antiochos, S. K. 2002, *ApJ*, 567, L97
 Aulanier, G., Srivastava, N., & Martin, S. F. 2000, *ApJ*, 543, 447
 Dahlburg, R. B., Antiochos, S. K., & Klimchuk, J. A. 1998, *ApJ*, 495, 485
 Démoulin, P., & Klein, K.-L. 2000, in *Transport and Energy Conversion in the Heliosphere*, ed. J.-P. Rozelot, L. Klein, & J.-C. Vial (Berlin: Springer), 99
 DeVore, C. R., & Antiochos, S. K. 2000, *ApJ*, 539, 954
 Karpen, J. T., Antiochos, S. K., Hohensee, M., Klimchuk, J. A., & MacNeice, P. J. 2001, *ApJ*, 553, L85
 Leka, K. D., Canfield, R. C., McClymont, A. N., & van Driel-Gesztelyi, L. 1996, *ApJ*, 462, 547
 Linker, J. A., Lionello, R., Mikić, Z., & Amari, T. 2001, *J. Geophys. Res.*, 106, 25165
 Lites, B. W., Low, B. C., Martinez Pillet, V., Seagraves, P., Skumanich, A., Frank, Z. A., Shine, R. A., & Tsuneta, S. 1995, *ApJ*, 446, 877
 Mandrini, C. H., van Driel-Gesztelyi, L., Thompson, B., Splunkett, A., Démoulin, P., & Aulanier, G. 2000, *Geofis. Inter.*, 39, 73
 Martin, S. F., Bilimoria, R., & Tracadas, P. W. 1994, in *Solar Surface Magnetism*, ed. R. J. Rutten & C. J. Schrijver (Dordrecht: Kluwer), 303
 Martin, S. F., & Echols, C. R. 1994, in *Solar Surface Magnetism*, ed. R. J. Rutten & C. J. Schrijver (Dordrecht: Kluwer), 339
 Martin, S. F., & McAllister, A. H. 1997, in *Coronal Mass Ejections*, ed. N. Crooker, J. A. Joselyn, & J. Feynman (Geophys. Monogr. 99; Washington, DC: AGU), 127
 Mok, Y., Schnack, D. D., & Van Hoven, G. 1991, *Sol. Phys.*, 132, 95
 Poland, A. I., & Mariska, J. T. 1986, *Sol. Phys.*, 104, 303
 Rosner, R., Tucker, W. H., & Vaiana, G. S. 1978, *ApJ*, 220, 643
 Serio, S., Peres, G., Vaiana, G. S., Golub, L., & Rosner, R. 1981, *ApJ*, 243, 288
 van Ballegooijen, A. A., & Martens, P. C. H. 1989, *ApJ*, 343, 971
 ———. 1990, *ApJ*, 361, 283
 Vesecky, J. F., Antiochos, S. K., & Underwood, J. H. 1979, *ApJ*, 233, 987
 Zirker, J. B., Engvold, O., & Martin, S. F. 1998, *Nature*, 396, 440